Title

An injectable bone marrow-like scaffold enhances T cell immunity after hematopoietic stem cell transplantation.

Journal

Nature biotechnology, 37(3)

ISSN

1087-0156

Authors

Shah, Nisarg J
Mao, Angelo S
Shih, Ting-Yu
et al.

Publication Date

2019-03-01

DOI

10.1038/s41587-019-0017-2

Peer reviewed

HHS Public Access

Author manuscript

Nat Biotechnol. Author manuscript; available in PMC 2019 August 11.

Published in final edited form as:

Nat Biotechnol. 2019 March ; 37(3): 293–302. doi:10.1038/s41587-019-0017-2.

An injectable bone marrow–like scaffold enhances T cell immunity after hematopoietic stem cell transplantation

Nisarg J. Shah[1,2,3,4,#], **Angelo S. Mao**[1,2], **Ting-Yu Shih**[1,2], **Matthew D. Kerr**[1,2,#], **Azeem Sharda**[3,4,5], **Theresa M. Raimondo**[1,2], **James C. Weaver**[2], **Vladimir D. Vrbanac**[7,8], **Maud Deruaz**[7,8], **Andrew M. Tager**[7,8], **David J. Mooney**[1,2,*], **David T. Scadden**[3,4,5,6,*]

[1]John A. Paulson School of Engineering and Applied Sciences, Harvard University, Cambridge MA 02138, USA

[2]Wyss Institute for Biologically Inspired Engineering, Harvard University, Cambridge, Massachusetts 02138, USA

[3]Department of Stem Cell and Regenerative Biology, Harvard University, Cambridge, MA 02138, USA

[4]Harvard Stem Cell Institute, Cambridge, MA 02138, USA

[5]Center for Regenerative Medicine, Massachusetts General Hospital, Boston, MA 02114, USA

[6]Cancer Center, Massachusetts General Hospital, Boston, MA 02114, USA

[7]Center for Immunology and Inflammatory Diseases, Massachusetts General Hospital, Harvard Medical School, Boston, MA 02114, USA.

[8]Ragon Institute of MGH, MIT and Harvard, Cambridge, MA 02139, USA

Abstract

The use of allogeneic hematopoietic stem cell transplantation (HSCT) to cure multiple disorders is limited by deficiency and dysregulation of T-cells. Here we report a biomaterial-based scaffold that mimics features of T-cell lymphopoiesis in the bone marrow. The bone marrow cryogel (BMC) releases bone morphogenetic protein-2 to recruit stromal cells, and presents the Notch ligand Delta-like ligand-4 to facilitate T-cell lineage specification of mouse and human hematopoietic progenitor cells. BMCs subcutaneously injected in mice at the time of HSCT enhanced T-cell progenitor seeding of the thymus, T-cell neogenesis and diversification of the T-

[*]Corresponding authors: David J. Mooney and David T. Scadden.

[#]Current address: Department of Nanoengineering, University of California, San Diego, La Jolla, CA 92093, USA.

Author contributions

N.J.S., A.S.M., D.T.S. and D.J.M. designed the experiments and analyzed the data. N.J.S, A.S.M., T.Y.S., M.D.K., A.S., J.C.W., V.D.V and T.M.R. conducted experiments. V.D.V., M.D. and A.M.T. assisted in analyzing the data. All authors provided input on the manuscript. N.J.S., A.S.M., D.J.M. and D.T.S. wrote and edited the paper.

Competing interests

The authors declare relevant competing financial interests as follows: Magenta Therapeutics, equity and consulting: D.T.S., Fate Therapeutics, equity and consulting: D.T.S., GlaxoSmithKline consulting and sponsored research: D.T.S. Novartis, sponsored research: D.J.M., Agnovos, consulting: D.J.M, Amgen, sponsored research: D.J.M., Samyang Corp., consulting: D.J.M. Decibel, sponsored research: D.J.M., Merck, sponsored research: D.J.M., Immulus, equity: D.J.M. Inventors, patent applications (PCT/US2017/016729), N.J.S, A.S.M., T.Y.S, D.J.M. and D.T.S.

cell receptor repertoire. Peripheral T-cell reconstitution increased ~6-fold in mouse HSCT and ~2-fold in human xenogeneic HSCT. Furthermore, BMCs promoted donor $CD4^+$ regulatory T-cell generation and improved survival after allogeneic HSCT. Compared with adoptive transfer of T-cell progenitors, BMCs increased donor chimerism, T-cell generation and antigen-specific T-cell responses to vaccination. BMCs may provide an off-the-shelf approach for enhancing T-cell regeneration and mitigating graft-versus-host disease in HSCT.

Introduction

T-cells are critical helper, effector and regulatory immune cells that are essential for life. Reduced T-cell numbers and functional deficiencies are causally implicated in diseases ranging from congenital immunodeficiency to autoimmune and impaired immune surveillance disorders [1, 2]. In allogeneic HSCT, there is a marked deficiency in T-cell generation, which renders patients susceptible to infectious agents and may contribute to graft-versus-host disease (GVHD)[3]. These complications can be fatal and limit the use of HSCT in settings where it can be curative. Balanced reconstitution of the naïve helper and effector T-cell subsets, along with the restoration of the T-cell receptor repertoire remains a significant unmet clinical need[4].

New T-cell regeneration from transplanted hematopoietic cells requires the availability of an adequate pool of T-cell progenitors[5] arising from bone marrow and adequate thymic function[6]. While there is currently no clinical standard for enhancing T-cell generation in vivo, most efforts have focused on using cytokines and cell-based therapies from the post-bone marrow phases of T-cell lymphopoiesis. However, in clinical trials, T-cell expansion cytokines IL-7 and IL-2[7] increased primarily mature T-cell subsets[8], and IL-2 was further limited by toxicity[9]. In contrast, the administration of IL-22 has been shown to enhance early thymocyte recovery in preclinical mouse studies[10]. Alternatively, adoptive donor T-cell infusion has been used to provide antigen-specific T cell protection against commonly encountered pathogens[11, 12], but has been associated with a transient response, increased risk of GVHD, and T-cell exhaustion. The above strategies are all limited by the availability of an adequate pool of T-cell progenitors to promote thymus-dependent T-cell generation. T-cell precursors can be robustly generated ex-vivo by the activation of Notch signaling, and co-administration of these cells with HSCT improves thymopoiesis and thymic architecture without exogenously co-administered cytokines [13–15]. However, ex-vivo cell culture to generate sufficient progenitors is laborious and only a transient enhancement in thymopoiesis of donor cells has been demonstrated. Thus, the widespread clinical translation of this approach would likely be complex.

Seeking to develop a broadly applicable technology, we focused on the pre-thymic bone marrow resident common lymphoid progenitors (CLPs), which have the capacity to differentiate into naïve T-lymphocytes when Notch signaling is activated, and are a major source of thymopoiesis[16–18]. The stromal component of the bone marrow niche that enhances T-cell lineage specification consists of osteocalcin-expressing bone marrow stromal cells producing delta-like ligand-4 (DLL-4), which provide a functional microenvironment critical for generating T-cell competent CLPs[19]. These stromal cells are

damaged by the process of pre-conditioning which likely impacts their T-cell lineage-instructive function. Additionally, the clinical experience with AIDS patients indicates that the adult thymus has the capacity to markedly improve in cellular composition and T-cell neogenesis despite prior dysfunction and atrophy[20]. These prior findings supported the development of a niche based on specific biologic aspects of T-cell lymphopoiesis in the bone marrow. We hypothesized that a T-cell lymphopoietic bone marrow niche might be engineered to foster production of T-cell progenitors in vivo that emigrate into the native thymus and thereby undergo host driven selection to create a more balanced and broad immune repertoire. We created an injectable, biomaterial-based bone marrow cryogel (BMC) scaffold that promotes T-cell development in vivo by integrating molecular signals that are presented in the bone marrow niche. The BMC comprises a macroporous hydrogel-based scaffold permitting cellular infiltration. It releases bone morphogenetic protein-2 (BMP-2) to facilitate the recruitment of host stromal cells and their osteolineage differentiation and presents bioactive Notch ligand DLL-4 at predefined densities to infiltrating hematopoietic cells. These T-lineage cues enhanced thymic seeding of progenitors and enabled donor T-cell reconstitution after syngeneic (syn) and allogeneic (allo) HSCT in mice. The BMC-reconstituted T-cells were functional, with a diverse T-cell receptor (TCR) repertoire, and reduced induction of GVHD.

Results

Macroporous Bone Marrow Cryogels (BMCs) differentiate hematopoietic progenitor cells in vitro

The scaffold-based Alginate-PEG BMC is a macroporous hydrogel with interconnected pores 50–80μm in diameter (Fig. 1a-c). DLL-4 was incorporated into the polymer backbone to promote the T-cell lineage program in hematopoietic progenitor cells[17]. To enable de novo bone formation[21], BMP-2 was added to the reaction mixture prior to cryo-polymerization for subsequent release in soluble form *in vivo*. These cryogels present both immobilized (DLL-4) and soluble (BMP-2) cues, unlike previous cryogels which were solely designed for controlled release of proteins[22]. In this work, the BMCs additionally support the growth of bone and hematopoietic tissue. I*n vitro* BMP-2 release (encapsulation efficiency 90%) displayed an initial burst of about 5% of the loaded amount, and then released in a sustained manner (Fig 1d). Less than 1% of the total loaded DLL4 was detected in the supernatant, and modified DLL-4 had similar binding kinetics to that of the unmodified protein (Fig. 1e). In the pooled release samples, over 90% of the bioactivity of the released BMP-2, relative to freshly reconstituted BMP-2 was retained (Supplementary Figure 1a). The bioactivity of BMP-2 ranged from 95% at Day 3 of release to ~85% at Day 12, confirming the released BMP-2 is highly active (Supplementary Figure 1b). The highest in vitro bioactivity of DLL-4 was found at the early time points, at Days 0 and 10 (Supplementary Figure 1c,d). The bioactivity decreased at subsequent time points but was still above baseline after 3 months. To measure the capacity of the BMC to induce the differentiation of hematopoietic progenitor mouse and human cells via Notch signaling, primary lineage depleted bone marrow cells from mice and cord-blood derived human $CD34^+$ hematopoietic cells were cultured in the BMC (Fig. 1f). The expansion of the common lymphoid progenitors saturated at 1% functionalization of the MA-COOH groups on the polymer backbone with

MA-DLL4, corresponding to approximately 6μg MA-DLL4 per gel and this condition was selected for further evaluation. There were no significant differences in the fold expansion and viability numbers of overall human or mouse cells in any of the experimental conditions analyzed (Supplementary Figure 1e, f). However, the fraction of lymphoid progenitor cells was enhanced only when DLL-4 was incorporated in the BMC, alone or in combination with BMP-2 (Fig. 1g).

BMCs form a bone nodule with features of hematopoietic tissue in vivo

The BMC was next analyzed for its ability to induce the trafficking of host and transplanted cells in a mouse model of HSCT. After lethal total body irradiation (L-TBI) mice were transplanted intravenously with lineage-depleted hematopoietic cells (5×10^4; ~93% lineage depleted, Supplementary Fig. 2a) isolated from donor mice bone marrow, and the BMCs (without cells) were simultaneously injected in the subcutaneous tissue of the dorsal flank (Fig. 2a). To grossly quantify cell infiltration in the BMCs, the size of each subcutaneous nodule was measured over a period of 6 weeks (Fig. 2b). In the BMC with BMP-2, nodule size rapidly increased to approximately 3 times over the initial volume after the first 10 days post-transplant and was substantially infiltrated with donor hematopoietic cells (Fig. 2c), forming a local bone nodule over a period of approximately 2 weeks, (Fig. 2d, e). Notably, bone formation was accompanied by vascularization, the DLL-4 remained accessible, and bone was restricted to the BMC scaffold, demonstrating the control afforded by the BMC over this process at an ectopic site (Fig. 2f-j, Supplementary Fig. 2b, Supplementary Note 1).

BMCs recruit and expand host stromal and transplanted hematopoietic cells

We assessed the infiltration and cell composition of the transplanted hematopoietic cells in the BMC at various time points post-transplant. The donor GFP^+ cells expanded when BMP-2 was included but not in the presence of DLL-4 alone (Fig. 3a, Supplementary Figure 2c). The stromal cells populating the BMCs and the native bone marrow were found to be similar, there was no difference in the engraftment of hematopoietic cells in native bone marrow of BMC-treated and non-treated mice, and SDF-1α and interleukin-7 concentrations were similar in the BMCs and native bone marrow (Supplementary Figure 2d-g, Supplementary Note 2). At the later time points (> 5 days post transplant), more primitive donor hematopoietic cells (HSCs and LMPPs) were quantified in the BMC. At Day 14, between 6 and 7 million total GFP^+ cells were quantified in the BMCs containing single factor BMP-2 or dual factor BMP-2 and DLL-4. Over 80% of cells were $CD11b^+$ myeloid cells in both groups. However, the CLP fraction in the transplanted donor cells expanded only within dual factor BMCs, resulting in a ~100-fold increase relative to BMCs with only BMP-2 at 2-weeks post-transplant (Fig. 3a). At 6-weeks post-transplant CLPs were ~10-fold higher in the dual factor BMCs, of which approximately 30% and 70% respectively were in the T-cell competent $Ly6D^-$ subset (Fig. 3b). Progenitor T-cells from the bone marrow migrate to the thymus to differentiate into naïve T-cells. To directly assess whether cells from the BMC migrate to the thymus, the dual factor BMC in concert with stem cell therapy was delivered into an initial set of lethally irradiated mice (Fig. 3c, d). The dual BMC was then explanted from these mice at day 10, and surgically transplanted into sublethally irradiated recipients subcutaneously in the dorsal flank. On day 20 post-BMC

transplantation, the donor GFP$^+$ and host cells in the thymus of these mice were quantified. GFP$^+$ DP, SP CD4$^+$ and SP CD8$^+$ cells were quantified in the thymus of BMC-transplanted recipient mice confirming migration of T-cell progenitor cells from the BMC to the thymus. In a separate study, Dual BMC treatment resulted in a greater enhancement of the number of ETPs in the thymus when compared to a 10-fold increase in the administered transplant cell dose without BMC (Fig. 3e). The Dual BMC also significantly outperformed bolus delivery of the factors placed in the BMC, and the BMP-2 only BMC, in generating thymocyte subsets over time (Fig. 3f-k, Supplementary Note 3).

BMCs enhance T-cell regeneration after HSCT and mitigate GVHD

In the peripheral blood of mice treated with the dual functionalized BMC, acceleration in T-cell reconstitution was observed approximately 4 weeks post-transplant, but no significant difference was observed in B-cell or myeloid cell reconstitution (Fig. 4a, Supplementary Fig. 3a, b). An analysis of T-cell subsets in the blood, spleen and bone marrow indicated that the homeostatic CD4$^+$:CD8$^+$ T-cell ratio was restored in mice with the dual functionalized BMCs after 30 days post-transplant in the spleen and bone marrow, and 40 days post-transplant in the peripheral blood (Fig. 4b-d). When the BMC treatment was used in the context of HSCT after sublethal total body irradiation (SL-TBI), there was enhanced T-cell reconstitution (Fig. 4e-j, Supplementary Figure 3c, d). At 28 days-post transplant the donor chimerism and absolute number of DP donor thymocytes were 1.5-fold and 2-fold higher respectively in BMC treated mice relative to mice that received just the transplant (Fig. 4e). There was also a higher donor chimerism and absolute number of donor-derived SP4 (by 2-fold and 3-fold respectively) and SP8 (by 1.7-fold and 15-fold respectively) thymocytes (Fig. 4f, g). In the periphery, the donor chimerism was higher in the CD4$^+$ (by 3.5-fold) and CD8$^+$ (by 2.5-fold) T-cells. No difference was observed in the chimerism or absolute number of B-cells.

We next assessed the rate of human T-cell reconstitution using an established xenogeneic NSG-BLT mouse model[23]. In BMC-treated NSG-BLT mice, there was an early enhancement in the initial rate of T-cell reconstitution, and a modest, transient reduction in the rate of B-cell reconstitution (Fig. 5a, b), with transiently fewer pre-B cell CFUs in the bone marrow of BMC-treated NSG-BLT mice (Supplementary Fig. 4). The peripheral CD4$^+$:CD8$^+$ T-cell ratio was stabilized in BMC-treated mice between 50 and 60 days post-transplant, whereas the CD4$^+$ compartment in control NSG-BLT was not fully reconstituted (Fig. 5c). Strikingly, the enhanced rate of T-cell reconstitution did not accelerate the rate of GVHD-related death. Instead, NSG-BLT mice that received the dual functionalized BMC survived longer than the NSG-BLT mice (Fig. 5d). In BMC-treated NSG-BLT mice, CD4$^+$FoxP3$^+$ regulatory T-cells (T_{reg}) were 2-fold higher in the thymus and spleen of BMC-treated mice at 50 days post-transplant in this model (Fig. 5e, Supplementary Figure 5a). A similar enhancement in survival was observed in an allogeneic MHC-mismatch HSCT mouse model that received the BMC (Figure 5f), and donor-derived CD4$^+$FoxP3$^+$ T_{reg} were 5-fold and 4-fold higher in the thymus and spleen, respectively, of BMC-treated mice 15 days post-transplant in this model (Fig. 5g).

We next compared our BMC treatment to a widely studied T-cell progenitor infusion approach, consisting predominantly of DN2 and DN3 precursors (> 90%) generated ex vivo using OP9-DL1 feeder cells (Supplementary Figure 5b). At 28 days post-HSCT, donor chimerism was significantly higher in the BMC-treated mice in the DP, SP4 and SP8 thymocyte populations (Figure 5h-j). In the spleen, donor chimerism was higher for both $CD4^+$ and $CD8^+$ T-cells, and higher absolute numbers of donor $CD4^+$ and $CD8^+$ T-cells were found with BMC-treatment (Figure 5k, l).

BMCs facilitate the enhancement of T-cell receptor diversity and function of regenerated T-cells

The diversity in T-cell receptors (TCR diversity) is produced by stochastic somatic recombination of gene segments in the thymus. In dual BMC treated mice, the thymus cellularity and the thymus weight were significantly higher than transplant-only controls upto ~6 weeks post-transplant (Supplementary Figure 6a, b). To characterize whether the increase in thymic cellularity also enhanced the functionality and diversity of the regenerated T-cells in syngeneic transplants, we quantified TCR excision circles (TRECs), which are a signature of TCR rearrangement, and conducted a TCR repertoire analysis. TREC number in the thymus of dual BMC-treated mice 1 month after transplantation were similar to that in non-irradiated control mice, and both were greater than in transplant only mice and BMP-2 BMC treated mice (Fig. 6a). In the spleen, an overall lower number of TRECs were noted in the same groups relative to the non-irradiated control, but mice treated with dual BMCs still had a higher TREC count relative to the transplant only and single factor BMP-2 BMC groups (Figure 6b). We next evaluated the diversity of the TCR V and J segments in the CDR3 beta chain of the BMC treated and transplanted mice 30 days post-HSCT using the Simpson's index (SI), which takes into account the number of T-cell clones present, as well as the relative abundance of each clone. The SI of mice with the dual functional BMC was 40% that of non-irradiated control mice, whereas the SI in mice administered the transplant alone or with BMP-2 BMC were lower (16% and 8%, respectively) (Fig. 6c). In HSCT, the lack of naive T cells with a broad TCR repertoire has been associated with increased risk of immunological complications and opportunistic infections[24]. The recovery of a greater number of TRECs in the thymus and periphery of dual BMC treated mice mirrors the enhancement in thymopoiesis. Relatively high frequencies of specific TCR clones were also observed in mice treated with dual BMCs, but a greater overall diversity suggested a more balanced thymus-derived reconstitution.

To measure the capacity of regenerated T-cells to respond in an antigen-specific manner, syngeneic transplants were vaccinated and subsequently challenged with a model protein ovalbumin (OVA) 30 days after transplantation (Fig. 6d). OVA epitope (SIINFEKL)-specific $CD8^+$ T-cells were significantly higher in mice that received the dual functional BMC, as compared to transplanted mice that did not receive the BMC or that received the BMC with BMP-2 only (Fig. 6e). Similarly, in dual BMC-treated mice that received the allogeneic transplant, the donor antigen-specific T-cell response was approximately 3-fold higher, as compared to that resulting from the pro-T-cell therapy approach (Fig. 6f). We found that the production of interferon (IFN)-γ and tumor necrosis factor–α (TNF-α) upon *ex vivo* stimulation was comparable for donor $CD4^+$ and $CD8^+$ T-cells in the BMC treatment and T-

cell progenitor treatment groups at Day 22, but a significantly greater fraction of T-cells from the BMC-treated group produced these factors at Day 42 (Fig. 6g-h). The robust antigen-specific generation of $CD8^+$ T-cells after vaccination in BMC treated mice post-HSCT suggests that the BMC treatment has the potential to be used in combination with post-HSCT vaccination.

Discussion

Here, we demonstrate that a cell-free biomaterial-based BMC mimicked key features of the T-cell lymphopoietic bone marrow niche and promoted the regeneration of immune competent T-cells after hematopoietic stem cell transplantation. Subcutaneously administered BMCs interfaced with the host vasculature to form a host-device interface and presented lineage-instructive cues to donor recruited progenitor cells in vivo. It is well established that BMP-2 induces osteolineage differentiation of recruited mesenchymal cells and indirectly promotes rapid neoangiogenesis[25]. In this work, we observed early neoangiogenesis, followed by maturation of the vasculature to densities consistent with those observed in endogenous bone marrow[26]. The finding of various hematopoietic and stromal progenitor populations quantified within the BMC are consistent with previous observations of hematopoiesis occurring within an ectopic bone nodule[27, 28]. The incorporation of bioactive Notch ligand DLL-4 on the polymer scaffold promoted an early enhancement in the generation of T-cell progenitors in the BMC and led to a significant increase in the number of thymic progenitors relative to controls receiving lineage-depleted bone marrow grafts, and the controls were consistent with established models of syngeneic- and allogeneic-HSCT[29, 30]. This finding is supported by the observation of enhanced generation of TRECs, the increased complexity of the TCR repertoire and the increased vaccination efficacy.

The BMC approach is distinct conceptually and in practice from other strategies to promote post-HSCT T-cell regeneration and its relevance in HSCT is supported by the preclinical studies in this work. It resulted in a higher number of T-cell progenitors and functional T-cells in the thymus and the periphery when used with a 10-fold lower dose relative to T-cell progenitor infusion. The BMC treatment varies from other methods in that it can be administered at the time of HSCT. In contrast, T-cell progenitors are produced in vitro from donor hematopoietic cells over 2–4 weeks, have complex cell culture requirements in pre-clinical models and are patient specific. By providing the T-cell promoting cues to the transplanted HSCs in vivo without the need for ex-vivo culture, the BMC approach may be an off-the-shelf product, avoid the considerable infrastructure needed for cell manufacturing [31] and may complement the activities of cytokine therapies. When a lower radiation dose was used prior to HSCT, the BMC modestly enhanced T-cell reconstitution in the periphery, but significantly increased donor-derived T-cell generation in the thymus and donor T-cell chimerism. The finding suggests the application of the BMCs will be relevant in settings of lower intensity HSCT.

The enhancement in the reconstitution of human T-cells in xenogeneic NSG-BLT mice was accompanied by a modest and transient reduction in B-cell reconstitution, consistent with a corresponding decrease in pre-B CFUs. While this humanized mouse model is widely

accepted for human immune cells, it is also known that key mouse cytokines are inefficient at inducing hematopoiesis including the development of human B-cells from human CD34$^+$ cells in this model[32]. It is likely that the Notch activation of the fraction of the transplanted cells, which seed the BMC enhances T cell specification at the expense of B cell specification. However, the transient reduction in B-cell production is modest and unlikely to be of clinical significance.

The formation of a bone nodule is restricted to the geometry of the scaffold, consistent with previous reports of scaffold-induced bone formation, which has been well tolerated in many species, including non-human primates[33] and in humans[34, 35]. Our clinical experience with other scaffold-based systems indicates that the size of the device may remain constant between species[36]. Even with the larger growth factor dose that may be necessary for use in humans, we anticipate that the controlled release provided by this polymer-based hydrogel system would allow one to use several orders of magnitude lower BMP-2 than is currently used in the clinic, as high doses have been associated with undesirable side effects[37]. After T-cell regeneration, the BMC may be readily removed similar to other devices that are often used in HSCT or made with biodegradable materials to resorb [38].

CD4$^+$ T-cell recovery after allogeneic HSCT is usually delayed, leading to an inversion of the normal CD4/CD8 ratio[39]. In BMC treated mice, there was a more balanced reconstitution of T-cells and an enhancement in donor CD4$^+$ regulatory T-cells (T_{reg}) in the thymus and the spleen of humanized and allogeneically transplanted mice. Given the key role of donor T_{reg} in GVHD suppression[40], BMC-mediated enhancement of donor T_{reg} generation likely contributed to the mitigation of GVHD-like pathology and the enhanced survival of mice, potentially through BMP-2 regulation of TGF-beta family proteins, which are key regulators of T_{reg} expansion[41]. Moreover, the time course in the allogeneic GVHD model is consistent with at least some of the BMC role being due to an effect on pre-existing T-committed or mature T cells.

In sum, these findings suggest that the BMC represents a simple to administer, off-the-shelf system that can enhance T cell regeneration after HSCT. If the BMC system performs similarly in a human context, it may be a means of abrogating the immunological complications and opportunistic infections that limit clinical application of potentially curative HSCT.

Methods

General methods and statistics.

Sample sizes for animal studies were based on prior work without the use of additional statistical estimations[42, 43]. Results were analyzed by using one-way ANOVA with a Tukey *post hoc* test using GraphPad Prism software. Where ANOVA was used, variance between groups was found to be similar by Bartlett's test. Survival curves were analyzed by using the log-rank (Mantel–Cox) test. Alphanumeric coding was used to blind pathology samples and blood counting.

Materials

UP LVG sodium alginate with high guluronate content was purchased from ProNova Biomedical; 2-morpholinoethanesulfonic acid (MES), sodium chloride (NaCl), sodium hydroxide (NaOH), N- hydroxysuccinimide (NHS), 1-ethyl-3-(3-dimethylaminopropyl)-carbodiimide hydrochloride (EDC), 2-aminoethyl methacrylate hydrochloride (AEMA) and acetone were purchased from Sigma-Aldrich. ACRL-PEG-NH_2 (3.5 kDa) and 4arm PEG Acrylate (10 kDa) were purchased from JenKem Technology.

Bone Marrow Cryogel (BMC) fabrication

The bone marrow cryogel was made following a previously described technique with some modifications[44]. Methacrylated alginate (MA-alginate) was prepared by reacting alginate with AEMA. Sodium alginate was dissolved in a buffer solution (0.6% (wt/vol), pH ~6.5) of 100 mM MES buffer. NHS and EDC were added to the mixture to activate the carboxylic acid groups on the alginate backbone followed by AEMA (molar ratio of NHS:EDC:AEMA=1:1.3:1.1), and the solution was stirred at room temperature (RT) for 24 h. The mixture was precipitated in acetone, filtered and dried in a vacuum oven overnight at RT. Alginate- PEG BMCs were synthesized by preparing a 2.5 wt% solution of MA-alginate and 4arm PEG Acrylate macromonomers (molar ratio MA-alginate: 4arm PEG Acrylate = 4:1) in deionized water and subsequently adding tetramethylethylenediamine (TEMED) (0.5% (wt/vol)) and ammonium persulfate (APS) (0.25% (wt/vol)). ACRYL-PEG-NH_2 was conjugated with the Delta-like ligand 4 (DLL-4) (R&D Systems) using carbodiimide chemistry (molar ratio of NHS:EDC:DLL4 = 1:1.3:1.1). BMP-2 (R&D Systems) was added to the polymer solution before cryopolymerization. All precursor solution was precooled to 4 °C to decrease the rate of polymerization before freezing. After addition of the initiator to the prepolymer solution, the solution was quickly transferred onto a precooled (−20 °C) Teflon mold. After overnight incubation, the gels were thawed and collected in petri dishes on ice. For scanning electron microscopy (SEM), BMCs were incubated in increasing concentration of freshly prepared ethanol solution (30, 50, 70, 90 and 100%) for 20 minutes each. BMCs were then incubated in hexamethyldisilazane (Electron Microscopy Sciences) for 10 min and dried in a desiccator/vacuum chamber for at least 1 hour prior to mounting them for SEM. Dried BMCs were adhered onto sample stubs using carbon tape and coated with a platinum/palladium in a sputter coater. Samples were imaged using secondary electron detection on a Carl Zeiss Supra 55 VP field emission scanning electron microscope (SEM).

Biomolecule release quantification

The stock concentration of the BMP-2 was known from the manufacturer and verified using ELISA. To determine the release kinetics encapsulation efficiency of BMP-2 and to confirm stable conjugation of DLL-4, the BMCs were incubated in 1ml of sterile PBS at 37 °C with shaking. Media was replaced periodically. Released agents in the supernatant were detected by ELISA (Peprotech). The samples were released until no more BMP-2 was detectable in the release medium. Subsequently, the cryogel was digested using at least 1000U of the enzyme Alginate Lyase. The digested product was analyzed for BMP-2 using ELISA. The

amounts of BMP-2 and DLL-4 in the cryogel and release medium were compared with the known amount of loaded BMP-2 and DLL-4 to calculate the encapsulation efficiency.

Biomolecule activity assays

Alkaline phosphatase activity assay for BMP-2 bioactivity—MC3T3-E1 Subclone 4 cells were used to conduct an alakaline phosphatase assay as previously described[45]. Cells were cultured under different experimental conditions: (1) growth medium, (2) differentiation medium supplemented with BMP-2 release from BMCs and (3) Native BMP-2.

Notch activation assay for DLL-4 bioactivity—To quantify the in vitro bioactivity of DLL-4 after exposure to serum proteins, which could deactivate this morphogen in vivo, a previously characterized Notch reporter cell line, CHO-K1 +2xHS4-UAS-H2B-Citrine-2xHS4 cH1 +hNECD-Gal4esn c9, a gift from M. Elowitz lab, was used[46, 47]. These cells were grown in Alpha MEM Earle's Salts (Irvine Scientific) supplemented with 10% Tet System Approved FBS (Clontech), 100 U/ml penicillin −100 ug/ml streptomycin – 0.292 mg/ml L-glutamine (Gibco), at 37ºC in the presence of 5% CO_2 under a humidified atmosphere. BMCs both with and without the DLL-4 were incubated in 96-well plates with the complete cell culture medium, without cells. At pre-determined time intervals (up to 3 months), twenty-thousand Notch reporter cells were seeded in the wells on the BMCs. After 24 hours, confocal microscopy was performed using a Zeiss LSM 710 confocal system. The colorimetric output in response to binding with Notch ligand DLL-4 was quantified and used as an indicator of DLL-4 bioactivity in the scaffold (Supplementary Figure 1c). In particular, the total YFP fluorescence of each cell in a field of view (50 – 100; 4–5 field of views encompassing over 80% of the gel surface) was calculated and background fluorescence was subtracted. The median YFP fluorescence was calculated and divided by the median fluorescence of the cells seeded on the BMCs without DLL-4 and reported.

Affinity determination by surface plasmon resonance—Dissociation constants of wild-type DLL4 and MA-DLL4 for Notch1 were determined by surface plasmon resonance using a BIAcore T200 instrument (GE Healthcare) as described previously[34]. Briefly, biotinylated, recombinant Notch1 were immobilized on a streptavidin coated sensor chip (GE Healthcare). Increasing concentrations of wild-type of methacrylated DLL4 proteins in buffer were flowed over the chip at 20°C. Binding and dissociation phases were performed at 10μl/min for 120 seconds and 60 seconds, respectively. Steady-state binding curves were fitted using the BIAcore evaluation software to a 1:1 Langmuir model to determine the K_d.

In vitro cell culture in Bone Marrow Cryogel (BMC)—Mouse BM cells were harvested from the limbs. Crushed tissue and cells were filtered through a 70-micron mesh. A single cell suspension was prepared by passing the cells once through a 20-gauge needle. Total cellularity was determined by counting cells using a hemacytometer. BM cells were depleted of mature immune cells (expressing CD3-ε, CD45R/B220, Ter-119, CD11b or Gr-1) by magnetic selection (BD Biosciences). We incubated cells with a mix of Pacific Blue-conjugated lineage antibodies (antibodies to CD3, NK1.1, Gr-1, CD11b, CD19, CD4 and CD8) and with Sca-1– and c-kit–specific antibodies. We isolated hematopoietic cells

($Lin^{-}Sca\text{-}1^{hi}c\text{-}kit^{hi}$) using a FacsAria cell sorter (BD). Sorted cells were ≥95% pure. Human cord-blood derived $CD34^{+}$ cells were purchased (Allcells) and expanded for seven days using expansion supplements (Stemcell Technologies). $CD34^{+}$ cells were isolated using a positive selection kit (StemCell Technologies). 96 well plates were pre-coated with Pluronic F127 (Sigma). Each BMC was individually placed in a well of the 96 well plate. Ten thousand mouse or human cells, isolated as described above were added to the same well in a 200μl volume of RPMI (with L-Glutamine) 1640 with 10% fetal bovine serum (FBS) and 1% of antibiotic and anti mycotic solution (containing penicillin, streptomycin and amphotericin B). For mouse cells, the media was supplemented with 10 ng/ml of stem cell factor (SCF; R&D Systems), 10 ng/mL FMS-like tyrosine kinase 3 ligand (Flt3L; R&D Systems) and 1 ng/mL interleukin-7 (IL-7; R&D Systems) with a 50% medium exchange step at day 2, 4 and 6. For human cells, the media was supplemented with 100 ng/mL SCF, 100 ng/mL Flt3L, 100 ng/mL TPO (R&D Systems), and 100 ng/mL IL-7 (R&D Systems). After one week of culture, cells were isolated by digesting the BMC with 1mg/ml Alginate Lyase (Sigma). The solution was passed through a 70-micron filter and cells were processed for FACS analysis as described below.

BM transplantation and blood analysis

All animal work was approved by the Harvard Institutional Animal Care and Use Committee and followed the National Institutes of Health guidelines and relevant ethical regulations. C57BL/6 (B6, $H\text{-}2^{b}$), BALB/c ($H\text{-}2^{d}$), C57BL/6 ($CD\ 45.1^{+}$), CByJ.B6-Tg(UBC-GFP)30Scha/J (GFP) and NSG mice (Jackson Laboratories) were female and between 6 and 8 weeks old at the start of the experiment. All mice within each experiment were age-matched and no randomization was performed. Pre-established criterion for animal omission was failure to inject desired cell dose in transplanted mice and death due to post-surgical complications in humanized mice. Health concerns unrelated to the procedure (e.g., malocclusion, severe dermatitis) were criteria for omission and euthanasia.

Transplant models

All TBI experiments were performed with a Cs-137 γ-radiation source. Sublethal-TBI (SL-TBI, B6 recipient), 1×500 cGy + 5×10^{5} lineage-depleted bone marrow cells; syngeneic HSCT (syn-HSCT, B6 recipient) 1×1000 cGy + 5×10^{4} to 5×10^{5} (as indicated in the figures) lineage depleted GFP BM cells; allogeneic-HSCT with GVHD (BALB/c MHC-mismatched recipient) 1×850 cGy + 5×10^{5} lineage depleted GFP BM cells + 1×10^{6} GFP splenocytes; allogeneic-HSCT without GVHD (BALB/c MHC-mismatched recipient) 1×850 cGy + 5×10^{5} lineage depleted GFP BM cells or 5×10^{6} in vitro generated GFP T-cell progenitors + 10^{3} syngeneic HSCs as described elsewhere without modification[48]. Humanized BLT (bone marrow−liver−thymus) mouse studies were conducted by the MGH and Ragon Institute Human Immune System Mouse Program, with Institutional IACUC approval as described previously[23]. BM cells for transplantation or analysis were harvested by crushing all limbs or one femur, respectively and processed as described above. While the mice were anesthetized, they received subcutaneous injections of two BMCs, which were suspended in 0.2 ml of sterile PBS, into the dorsal flank by means of a 16-gauge needle. One BMC was injected on each side of the spine and positioned approximately midway between the hind and forelimbs. Subcutaneous nodule size was quantified over time by measuring the

nodule length, width and height using a caliper. All cohorts of mice (typically 10 mice/group) were serially bled. White blood cell, hemoglobin, red blood cell, platelet, and hematocrit levels were quantified by CBC analysis (Abaxis VetScan HM5).

For directly assessing whether cells from the BMC migrate to the thymus, the dual factor BMC in concert with stem cell therapy was delivered into an initial set of lethally irradiated mice (B6 recipients receiving 1000 cGy L-TBI and 5×10^5 lineage depleted GFP BM cells with dual factor BMC. 10-days post-HSCT, the dual factor BMC was explanted and immediately surgically transplanted in the subcutaneous pocket of a second set of B6 mice which had received 500 cGy SL-TBI 48-hours prior without any additional cell transplantation. 20-days post surgery, mice were sacrificed and the thymocytes were analyzed in these mice.

Flow cytometry (FACS) analysis

Anti-mouse antibodies to CD8-α (53–6.7), CD3-ε (145–2C11), B220 (RA3–6B2), CD11b (M1/70), CD25 (PC61), CD117 (2B8), Sca-1 (D7), CD127 (A7R34), and anti-human antibodies to CD45 (H130), CD3 (HIT3a), CD4 (SK3), CD19 (HIB19), CD34 (581), CD38 (HB-7) and CD7 (CD7–6B7), IFN-γ (XMG1.1), TNF-α (MP6-XT22) and the corresponding isotype antibodies were purchased from BioLegend. Anti-human CD8 (RPA-T8) was purchased from BD Biosciences. CD44 (IM7) was purchased from eBioscience. SIINFEKL tetramer (Alexa Fluor 647 H-2K^b OVA) were obtained from the NIH Tetramer Core Facility. All cells were gated based on forward and side-scatter characteristics to limit debris including dead cells. Antibodies were diluted according to the manufacturer's suggestions. Cells were gated based on fluorescence minus one controls, and the frequencies of cells staining positive for each marker was recorded. For quantifying T, B, and myeloid cells, blood samples were red blood cell–lysed and stained with anti-CD45, -B220, -CD3, -CD4, -CD8, and –CD11b antibodies, and absolute numbers of T, B, and myeloid cells were calculated using flow cytometry frequencies and white blood cell values obtained by CBC analysis. Analysis was based on donor events within the CD45$^+$ for blood cells and the CD45$^-$ gate for stromal cells.

Bone, Fat Quantification and Histology

After euthanasia, BMCs and tissues were explanted. For quantification of bone using bone alkaline phosphatase (BALP), the BMCs and femurs were crushed and homogenized and strained through a 70 micron filter. Subsequently, a BALP ELISA kit (Creative Diagnostics) was used to quantify the BALP by following the manufacturer's protocol. Oil Red O staining kit (Biovision) was used for lipid quantification. Harvested BMCs and bones were washed, fixed, processed and stained following the manufacturer's protocol. BMCs and bone were subsequently crushed, strained and resuspended in equal volumes before measuring absorbance (OD_{492}). For histological staining, tissues were fixed in 4% paraformaldehyde (PFA). PFA-fixed samples were partially decalcified for about 4 hours using a rapid decalcifying formic acid/hydrochloric acid mixture (Decalcifying Solution, VWR) and embedded in paraffin wax. Sections (5 μm) of the samples were stained with routine trichrome, Safranin-O or Verhoeff–Van Gieson stain.

Quantification of thymic T-cell receptor excision circles (TRECs).

TREC quantification was performed as previously described[35]. Briefly, thymi were harvested from non-irradiated C57BL/6 mice, transplanted mice, and transplanted mice with the injected BMC (30 d after conditioning). Total DNA was extracted using TRIZOL following tissue homogenization in a Bullet Blender Storm BBX24 instrument (Next Advance, Inc.). DNA was quantified by UV-Vis and 1 μg of DNA per sample was used as input for real-time PCR. A standard curve of mouse sjTREC plasmid was used to calculate the absolute number of single joint TRECS (sjTRECs) per sample.

TCR analysis

Extracted lymphocyte RNA was quantified using UV-Vis. Equimolar amounts of RNA from each sample was submitted to iRepertoire for sequencing and bioinformatics analysis, where samples were reverse transcribed and amplified using a primer set which specifically amplifies beta TCR RNA. The results of the sequencing gave a range of total reads and numbers of unique CDR3s for each sample.

Vaccination and non-specific T-cell-stimulation study

30 days after transplantation, animals were immunized with a bolus vaccine containing 100 μg ovalbumin (OVA), 100 μg CpG-ODN and 1 μg GM-CSF. After 10 d, animals were challenged with an intravenous injection of ovalbumin. On Day 12, spleens were collected from euthanized mice in the vaccination studies. Splenocytes were isolated by mechanical disruption of the spleen against 70-μm cell strainers. Red blood cells in the harvested tissues were lysed and leukocytes were prepared for analysis. For unspecific stimulation, cells were incubated for 5 h with PMA (10 ng/mL) + ionomycin (2 μM). Brefeldin A (10 μg/mL) was added after 2 h of incubation. The cells were then harvested, washed, and stained with fluorochrome-conjugated antibodies to T-cell surface antigens. Subsequently, cell were fixed and permeabilized with fixation/permeabilization solution kit reagents (BD) and stained with IFN-γ, TNF-α-specific antibodies.

Supplementary Material

Refer to Web version on PubMed Central for supplementary material.

Acknowledgments

The authors acknowledge helpful discussions with R. Yusuf and the Harvard Catalyst Biostatistical Consulting Program funded by the National Institutes of Health (UL1 TR001102). N.J.S was supported by the Cancer Research Institute-Gould Family Foundation Postdoctoral Fellowship. The work was supported by the National Institutes of Health through grants U19 HL129903 and R01 EB023287, and by the Blavatnik Biomedical Accelerator Program at Harvard University.

References

1. Goronzy JJ & Weyand CM Successful and maladaptive T cell aging. Immunity 46, 364–378 (2017). [PubMed: 28329703]
2. Liston A, Enders A & Siggs OM Unravelling the association of partial T-cell immunodeficiency and immune dysregulation. Nature Reviews Immunology 8, 545–558 (2008).

3. Blazar BR, Murphy WJ & Abedi M Advances in graft-versus-host disease biology and therapy. Nature Reviews Immunology 12, 443–458 (2012).
4. Krenger W, Blazar BR & Holländer GA Thymic T-cell development in allogeneic stem cell transplantation. Blood 117, 6768–6776 (2011). [PubMed: 21427289]
5. Zlotoff DA et al. Delivery of progenitors to the thymus limits T-lineage reconstitution after bone marrow transplantation. Blood 118, 1962–1970 (2011). [PubMed: 21659540]
6. Chaudhry MS, Velardi E, Dudakov JA & Brink MR Thymus: the next (re) generation. Immunological reviews 271, 56–71 (2016). [PubMed: 27088907]
7. Mohtashami M, Shukla S, Zandstra P & Zúñiga-Pflücker JC in Synthetic Immunology 95–120 (Springer, 2016).
8. Perales M-A et al. Recombinant human interleukin-7 (CYT107) promotes T-cell recovery after allogeneic stem cell transplantation. Blood 120, 4882–4891 (2012). [PubMed: 23012326]
9. Skrombolas D & Frelinger JG Challenges and developing solutions for increasing the benefits of IL-2 treatment in tumor therapy. Expert review of clinical immunology 10, 207–217 (2014). [PubMed: 24410537]
10. Dudakov JA et al. Interleukin-22 drives endogenous thymic regeneration in mice. Science, 1218004 (2012).
11. Cobbold M et al. Adoptive transfer of cytomegalovirus-specific CTL to stem cell transplant patients after selection by HLA–peptide tetramers. Journal of Experimental Medicine 202, 379–386 (2005). [PubMed: 16061727]
12. Rooney CM et al. Infusion of cytotoxic T cells for the prevention and treatment of Epstein-Barr virus–induced lymphoma in allogeneic transplant recipients. Blood 92, 1549–1555 (1998). [PubMed: 9716582]
13. Zakrzewski JL et al. Tumor immunotherapy across MHC barriers using allogeneic T-cell precursors. Nature biotechnology 26, 453 (2008).
14. Van Coppernolle S et al. Functionally mature CD4 and CD8 TCRαβ cells are generated in OP9-DL1 cultures from human CD34+ hematopoietic cells. The Journal of Immunology 183, 4859–4870 (2009). [PubMed: 19801512]
15. Awong G et al. Human proT-cells generated in vitro facilitate hematopoietic stem cell-derived T-lymphopoiesis in vivo and restore thymic architecture. Blood 122, 4210–4219 (2013). [PubMed: 24215033]
16. Love PE & Bhandoola A Signal integration and crosstalk during thymocyte migration and emigration. Nature Reviews Immunology 11, 469 (2011).
17. Radtke F, MacDonald HR & Tacchini-Cottier F Regulation of innate and adaptive immunity by Notch. Nature Reviews Immunology 13, 427 (2013).
18. Serwold T, Ehrlich LIR & Weissman IL Reductive isolation from bone marrow and blood implicates common lymphoid progenitors as the major source of thymopoiesis. Blood 113, 807–815 (2009). [PubMed: 18927436]
19. Vionnie W et al. Specific bone cells produce DLL4 to generate thymus-seeding progenitors from bone marrow. Journal of Experimental Medicine, jem. 20141843 (2015).
20. Smith KY et al. Thymic size and lymphocyte restoration in patients with human immunodeficiency virus infection after 48 weeks of zidovudine, lamivudine, and ritonavir therapy. The Journal of infectious diseases 181, 141–147 (2000). [PubMed: 10608760]
21. Wozney JM et al. Novel regulators of bone formation: molecular clones and activities. Science 242, 1528–1534 (1988). [PubMed: 3201241]
22. Koshy ST, Zhang DK, Grolman JM, Stafford AG & Mooney DJ Injectable nanocomposite cryogels for versatile protein drug delivery. Acta biomaterialia 65, 36–43 (2018). [PubMed: 29128539]
23. Brainard DM et al. Induction of robust cellular and humoral virus-specific adaptive immune responses in human immunodeficiency virus-infected humanized BLT mice. Journal of virology 83, 7305–7321 (2009). [PubMed: 19420076]
24. Douek DC et al. Assessment of thymic output in adults after haematopoietic stemcell transplantation and prediction of T-cell reconstitution. The Lancet 355, 1875–1881 (2000).

25. Smadja DM et al. Bone morphogenetic proteins 2 and 4 are selectively expressed by late outgrowth endothelial progenitor cells and promote neoangiogenesis. Arteriosclerosis, thrombosis, and vascular biology 28, 2137–2143 (2008).
26. Lafage-Proust M-H et al. Assessment of bone vascularization and its role in bone remodeling. BoneKEy reports 4 (2015).
27. Kuznetsov SA et al. The interplay of osteogenesis and hematopoiesis: expression of a constitutively active PTH/PTHrP receptor in osteogenic cells perturbs the establishment of hematopoiesis in bone and of skeletal stem cells in the bone marrow. J Cell Biol 167, 1113–1122 (2004). [PubMed: 15611335]
28. Song J et al. An in vivo model to study and manipulate the hematopoietic stem cell niche. Blood 115, 2592–2600 (2010). [PubMed: 20110425]
29. Wils E-J et al. Flt3 ligand expands lymphoid progenitors prior to recovery of thymopoiesis and accelerates T cell reconstitution after bone marrow transplantation. The Journal of Immunology 178, 3551–3557 (2007). [PubMed: 17339451]
30. Maillard I et al. Notch-dependent T-lineage commitment occurs at extrathymic sites following bone marrow transplantation. Blood 107, 3511–3519 (2006). [PubMed: 16397133]
31. Garber K. Driving T-cell immunotherapy to solid tumors. Nat. Biotechnol 36, 215–219 (2018). [PubMed: 29509745]
32. Jangalwe S, Shultz LD, Mathew A & Brehm MA Improved B cell development in humanized NOD-scid IL2Rγnull mice transgenically expressing human stem cell factor, granulocyte-macrophage colony-stimulating factor and interleukin-3. Immunity, inflammation and disease 4, 427–440 (2016).
33. Ripamonti U Bone induction by recombinant human osteogenic protein-1 (hOP-1, BMP-7) in the primate Papio ursinus with expression of mRNA of gene products of the TGF-β superfamily. Journal of cellular and molecular medicine 9, 911–928 (2005). [PubMed: 16364199]
34. Heliotis M, Lavery K, Ripamonti U, Tsiridis E & Di Silvio L Transformation of a prefabricated hydroxyapatite/osteogenic protein-1 implant into a vascularised pedicled bone flap in the human chest. International journal of oral and maxillofacial surgery 35, 265–269 (2006). [PubMed: 16257511]
35. Warnke P et al. Growth and transplantation of a custom vascularised bone graft in a man. The Lancet 364, 766–770 (2004).
36. ClinicalTrials.gov. Dendritic cell activating scaffold in melanoma. https://clinicaltrials.gov/ct2/show/NCT01753089
37. Carragee EJ, Hurwitz EL & Weiner BK A critical review of recombinant human bone morphogenetic protein-2 trials in spinal surgery: emerging safety concerns and lessons learned. The Spine Journal 11, 471–491 (2011). [PubMed: 21729796]
38. Biffi R et al. Use of totally implantable central venous access ports for high-dose chemotherapy and peripheral blood stem cell transplantation: results of a monocentre series of 376 patients. Annals of oncology 15, 296–300 (2004). [PubMed: 14760125]
39. Li MO & Rudensky AY T cell receptor signalling in the control of regulatory T cell differentiation and function. Nature Reviews Immunology 16, 220 (2016).
40. Hoffmann P, Ermann J, Edinger M, Fathman CG & Strober S Donor-type CD4+ CD25+ regulatory T cells suppress lethal acute graft-versus-host disease after allogeneic bone marrow transplantation. Journal of Experimental Medicine 196, 389–399 (2002). [PubMed: 12163567]
41. Wan YY & Flavell RA 'Yin–Yang'functions of transforming growth factor-β and T regulatory cells in immune regulation. Immunological reviews 220, 199–213 (2007). [PubMed: 17979848]
42. Bencherif SA et al. Injectable cryogel-based whole-cell cancer vaccines. Nature communications 6, 7556 (2015).
43. Palchaudhuri R et al. Non-genotoxic conditioning for hematopoietic stem cell transplantation using a hematopoietic-cell-specific internalizing immunotoxin. Nature biotechnology 34, 738 (2016).
44. Bencherif SA et al. Injectable preformed scaffolds with shape-memory properties. Proceedings of the National Academy of Sciences of the United States of America 109, 19590–19595 (2012). [PubMed: 23150549]

45. Macdonald ML et al. Tissue integration of growth factor-eluting layer-by-layer polyelectrolyte multilayer coated implants. Biomaterials 32, 1446–1453 (2011). [PubMed: 21084117]

46. Sprinzak D et al. Cis-interactions between Notch and Delta generate mutually exclusive signalling states. Nature 465, 86 (2010). [PubMed: 20418862]

47. Nandagopal N et al. Dynamic ligand discrimination in the Notch signaling pathway. Cell 172, 869–880. e819 (2018). [PubMed: 29398116]

48. Zakrzewski JL et al. Adoptive transfer of T-cell precursors enhances T-cell reconstitution after allogeneic hematopoietic stem cell transplantation. Nature medicine 12, 1039 (2006).

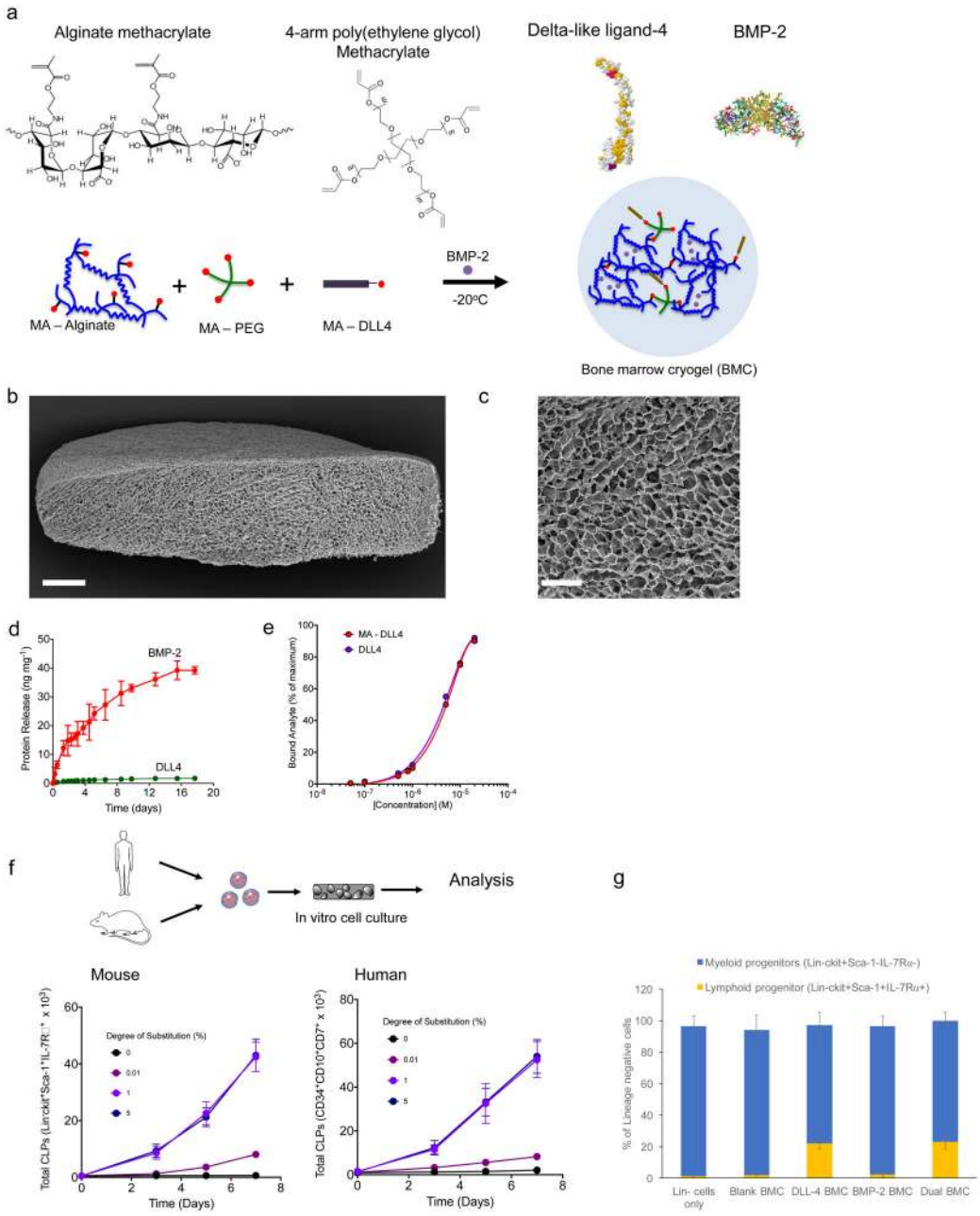

Figure 1.

Alginate-PEG-DLL4 based bone marrow cryogel (BMC) presents DLL4 and BMP-2, and preferentially expands common lymphoid progenitors (CLPs). (a) Schematic for the fabrication of covalently crosslinked BMC. (b) Representative cross sectional scanning electron micrograph (SEM) image of a BMC. Scale bar, 1mm. (c) Representative SEM of the pore shape and structure within the cross section of the BMC. Scale bar = 200μm. (d) Release kinetics of the encapsulated BMP-2 (red line) and covalently tethered DLL4 (green line) (n=5 per group) (e) Surface plasmon resonance measuring the binding kinetics of the DLL4 before and after modification with the methacrylate linker. (f) In vitro differentiation of isolated mouse and human hematopoietic stem and progenitor cells into CLPs as a

function of the degree of functionalization of methacrylate groups on the polymer backbone (n = 5). (g) Proportion of Lin^- common lymphoid and myeloid mouse progenitor cells quantified in growth medium, blank, single factor and dual factor BMCs. Images and pore size quantification in b, c are representative of ten independent replicates. Data in d, f, g represent the mean ± s.d. of five experimental replicates and are representative of three independent experiments. Distinct samples were assayed individually.

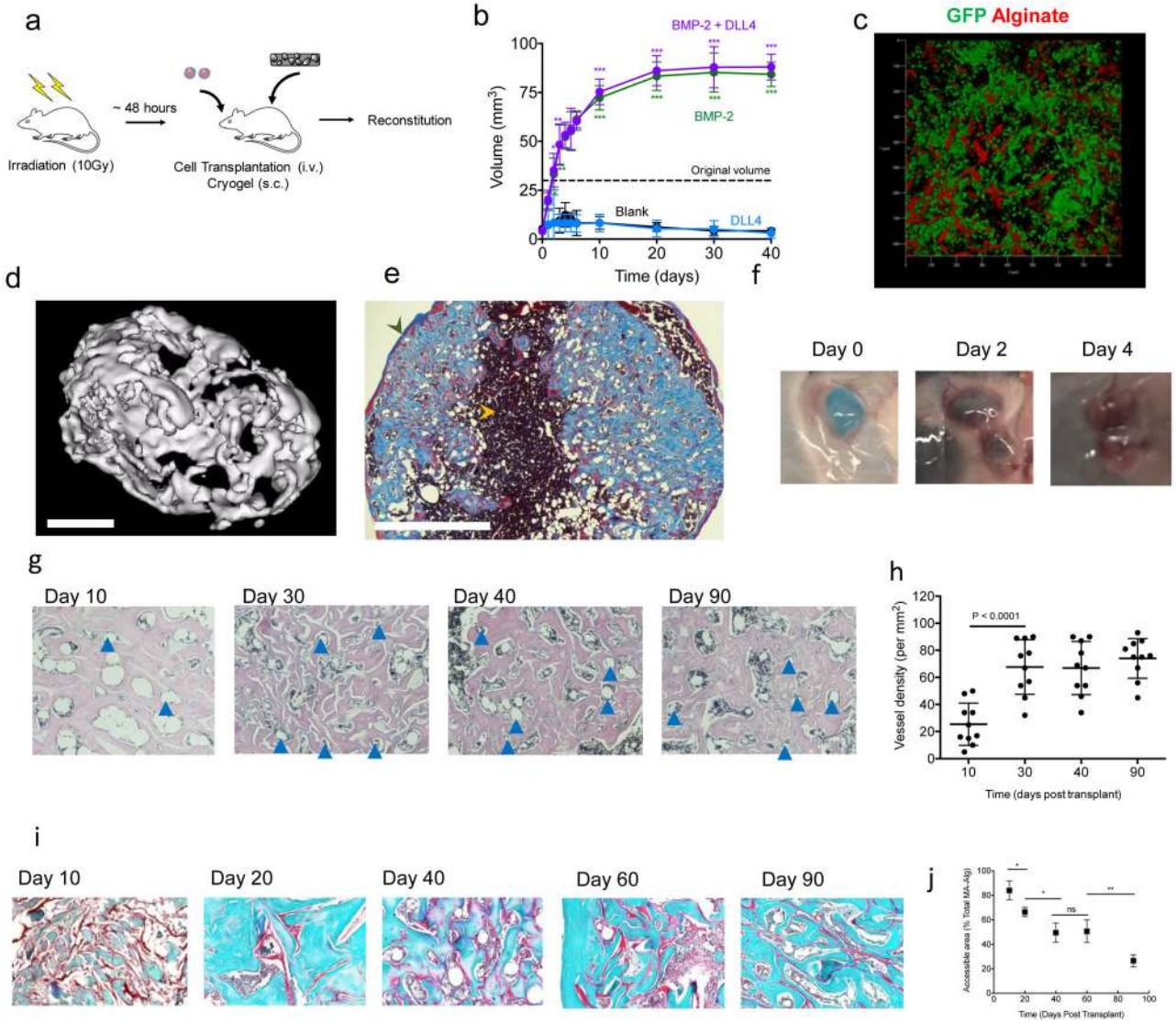

Figure 2.

In vivo deployment and host integration of BMCs. (a) Schedule of administration of L-TBI, HSCT and simultaneous injection of the BMCs. B6 mice were irradiated with 1000 cGy (1 dose) and subsequently transplanted with 5×10^5 lineage depleted syngeneic GFP BM cells within 48 hours after L-TBI. (b) The volume of the BMC nodule in vivo as a function of time post-delivery with various combinations of the BMP-2 and DLL-4 included in the BMC. (c) Confocal microscopy image of donor GFP+ cells (green) identified within the BMC (red) (d) Representative microcomputed tomography (microCT, scale bar = 1mm) imaging and (e) histology (scale bar = 1mm) of the dual functionalized BMC at 3 weeks post injection with the bone shell (green arrow) and the hematopoietic tissue (yellow arrow). (f) Images of the BMC (blue) in the subcutaneous tissue at various timepoints post-injection. (g) Histological Verhoeff–Van Gieson stained sections of the BMC with blood vessels identified (blue arrows) at Day 10, 30, 40 and 90 post-transplant and (h) quantification of the blood vessel density within these sections. (i) Histological Safranin-O stained sections of the

BMC with alginate identified (red thread-like staining) at Day 10, 20, 40, 60 and 90 post-transplant and (j) quantification of the accessible area of alginate within these sections. Data in b represent the mean ± s.d. of five experimental replicates and are representative of two independent experiments. (*P < 0.05, ** P < 0.01, ***P < 0.001, analysis of variance (ANOVA) with a Tukey post hoc test). Images in c-g, i are representative of four independent samples. Data in h, j represent the mean ± s.d. from eight samples and are representative of two independent experiments. Distinct samples were assayed individually.

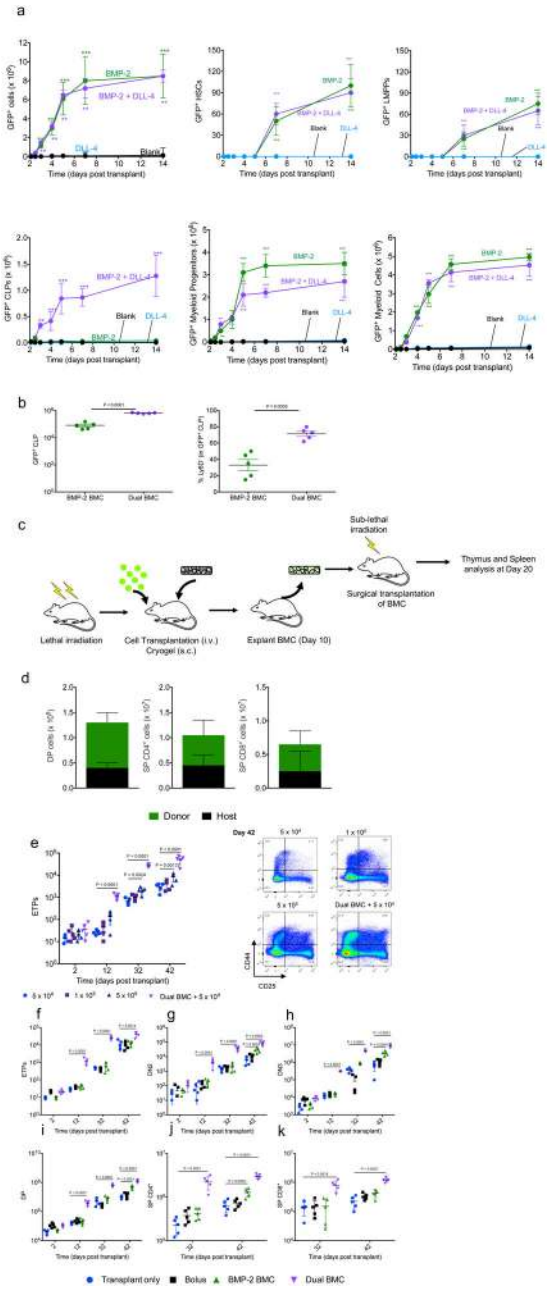

Figure 3.

In vivo recruitment of donor cells to BMC and enhanced seeding of thymic progenitors. (a) Total number and type of donor derived, GFP$^+$ cells in the BMC containing combinations of BMP-2 and DLL-4 and blank BMCs. (b) Absolute number of donor GFP$^+$ CLPs and the percentage of Ly6D$^-$ CLPs in BMP-2- and dual factor- BMCs. (c) Schematic of experimental setup for surgical transplantation of harvested BMCs from post-HSCT mice into sub-lethally irradiated mice. (d) DP, SP CD4$^+$ and SP CD8$^+$ cells quantified in the thymus 20-days post surgical transplantation of BMC. (e) Total number of early T-lineage progenitors (ETP; CD44$^+$CD25$^-$c-kit$^+$) quantified as a function of lineage-depleted transplanted cell dose compared with BMC treatment with the lowest cell dose at multiple

time points post transplant with representative FACS plots (five experimental replicates at each time point, 2 independent experiments). (f-k) Total number of early T-lineage progenitors (ETP; $CD44^{+}CD25^{-}c\text{-}kit^{+}$), DN2 ($CD44^{+}CD25^{-}$), DN3 ($CD44^{+}CD25^{-}$), DP, SP4, SP8 thymocyte subsets compared across different treatment conditions at multiple time points post transplant. For a, b, f-k the mice were transplanted with 5×10^5 lineage depleted syngeneic GFP BM cells within 48 hours after L-TBI (1 × 1000 cGy). In c, d an initial set of mice were transplanted with 5×10^5 lineage depleted syngeneic GFP BM cells within 48 hours after L-TBI. A subsequent set of mice received SL-TBI (1 × 500 cGy) without a subsequent cell transplant. In e, the mice were transplanted with 5×10^4 to 5×10^5 lineage depleted GFP cells. All groups are compared with transplant only control (*P < 0.05, ** P < 0.01, ***P < 0.001, analysis of variance (ANOVA) with a Tukey post hoc test). Data in a represents the mean ± s.d. of ten mice per group and are representative of two independent experiments. Data in b, d-k represent the mean ± s.d. from five mice per group, and at each time point in d-k and are representative of at least two independent experiments. In a all groups are compared with the blank gel control group. Comparisons are with the lowest cell dose group in e and the transplant only group in d-k. (*P < 0.05, ** P < 0.01, ***P < 0.001, analysis of variance (ANOVA) with a Tukey post hoc test). Distinct samples were assayed individually.

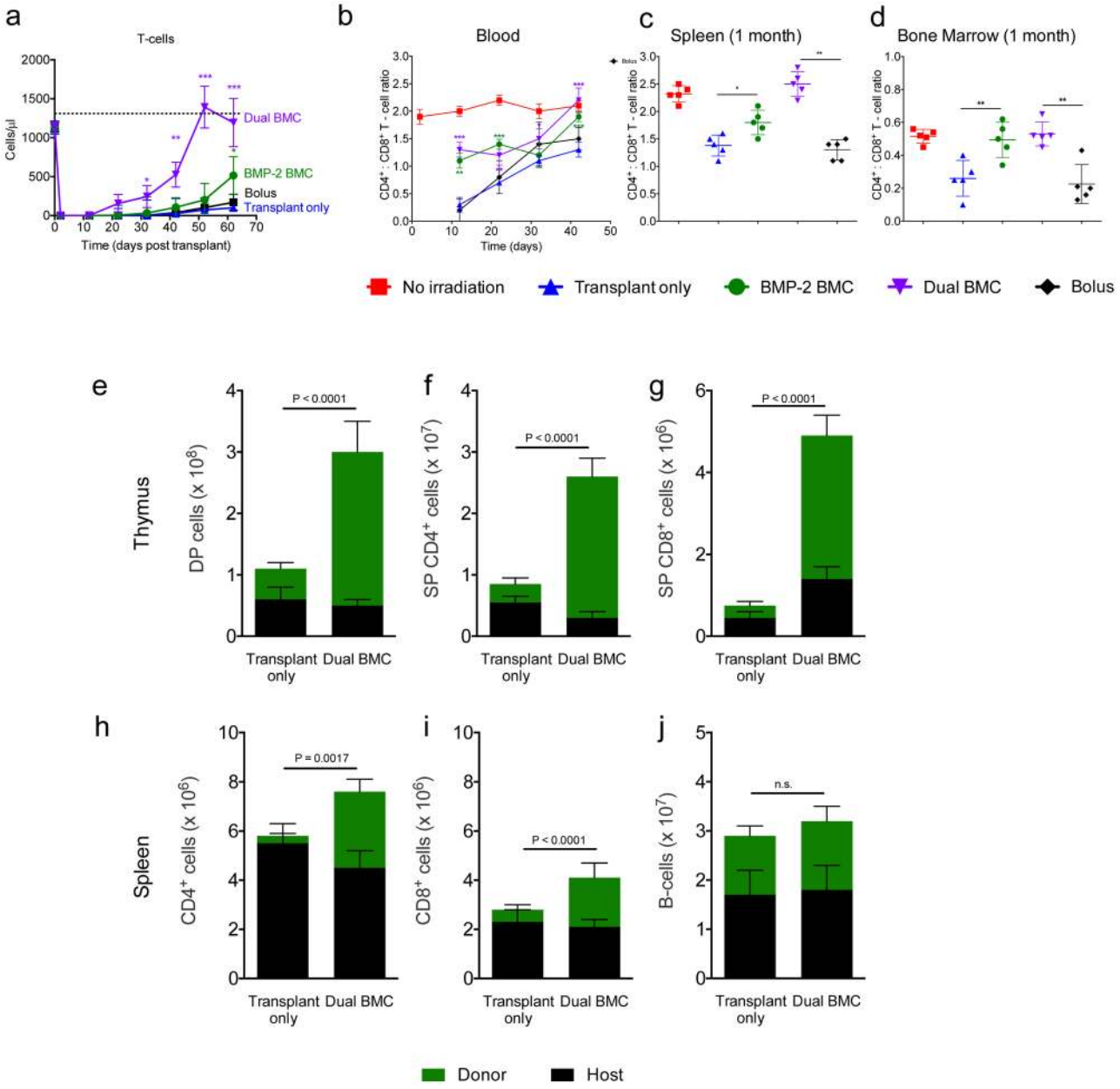

Figure 4.

Enhancement of T-cell reconstitution mediated by the BMC (a) The sum of $CD3^+CD4^+$ and $CD3^+CD8^+$ in the peripheral blood of mice post-HSCT. B6 mice were irradiated with 1 × 1000 cGy L-TBI dose. Mice were subsequently transplanted with 5×10^5 lineage depleted syngeneic GFP BM cells within 48 hours after L-TBI and treated as indicated in the figure. Measurement of the recovery in $CD4^+$ to $CD8^+$ T-cell ratios in the (b) blood, (c) spleen and (d) bone marrow, as a function of time, with non-irradiated mice as for comparison for the same groups as in (a). In (a - d) Post-HSCT mice with no BMC (Transplant only), post-HSCT mice treated with bolus BMP-2 and DLL-4 injection, a BMC containing BMP-2 (BMP-2 BMC), and post-HSCT mice treated with a BMC containing BMP-2 and DLL4 (Dual BMC) were analyzed. In (e-j) B6 mice were irradiated with 500 cGy SL-TBI and

subsequently transplanted with 5×10^5 lineage-depleted bone marrow cells within 48 hours post-radiation. Total number of (e) DP (f) SP4 and (g) SP8 thymocytes and peripheral (h) $CD4^+$ and (i) $CD8^+$ T-cells and (j) B-cells in the spleens of SL-TBI syn-HSCT mice that were treated with and without a dual BMC 28 days post-transplant. Data in a-d represent the mean ± s.d. of n = 8 mice per group for each time point and are representative of at least 3 independent experiments. Data in e-j represent the mean ± s.d. of n= 10 mice and are representative of 2 independent experiments. (*P < 0.05, ** P < 0.01, ***P < 0.001, analysis of variance (ANOVA) with a Tukey post hoc test).

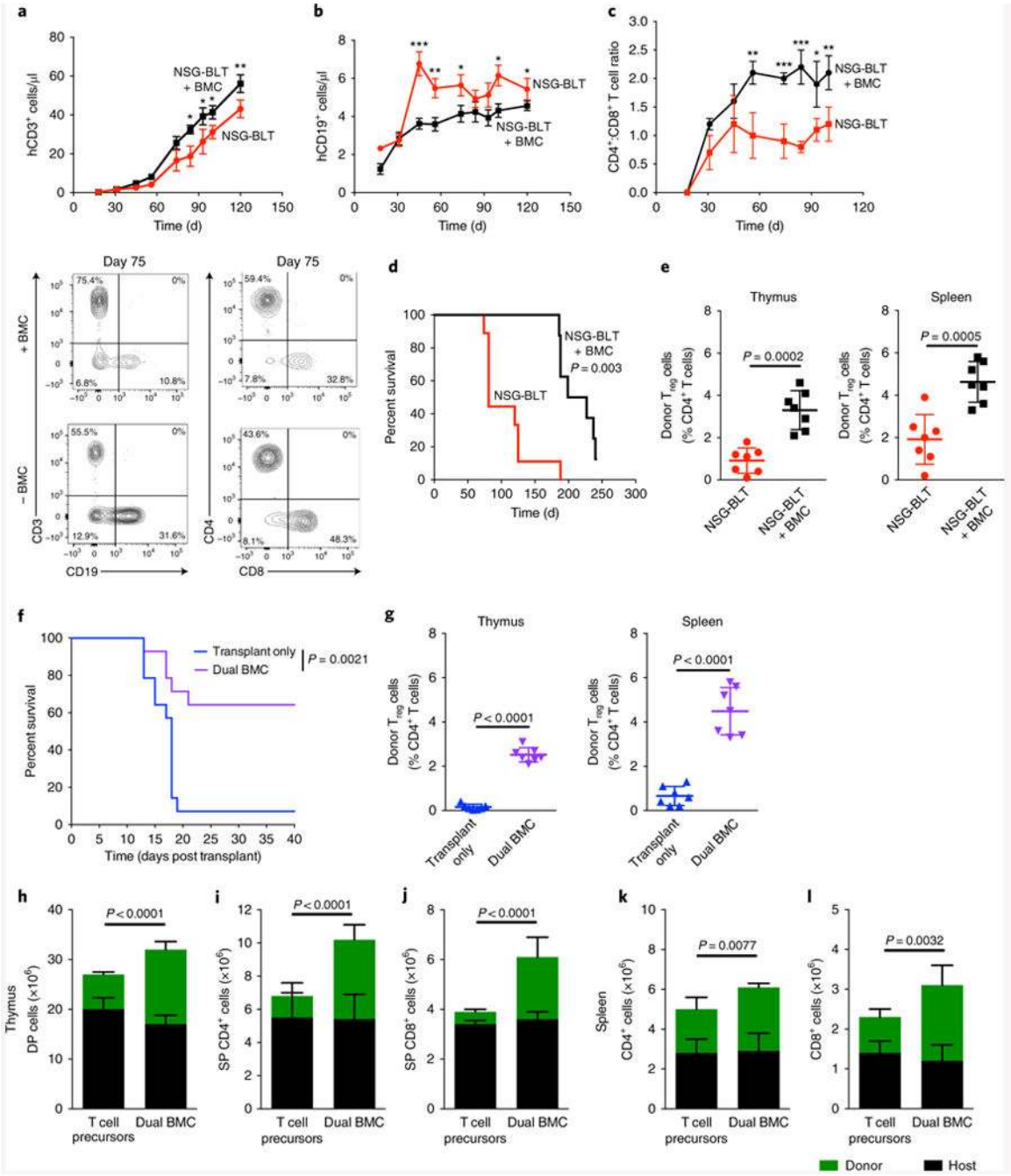

Figure 5.

Enhanced reconstitution of T-cells and mitigation of GVHD in NSG-BLT mice and in mice after allogeneic HSCT. Reconstitution of (a) $CD3^+$ T-cells and (b) $CD19^+$ B-cells with (c) $CD4^+$:$CD8^+$ ratio in humanized NSG-BLT mice with exemplary flow cytometry plots at day 75. (d) Survival rate in NSG-BLT mice (n = 10 per group) and (e) Reconstitution of human regulatory T-cells in the thymus and spleen of NSG-BLT mice with representative flow cytometry plots. In (a) through (e) xenogeneic humanized BLT (bone marrow−liver−thymus) mice were generated and used as described previously[23]. Mice with no BMC

(NSG-BLT) and mice with the Dual BMC (NSG-BLT + Dual BMC) with human donor tissue from the same source were analyzed. (f) Survival rate and (g) reconstitution of donor-derived regulatory T-cells in the thymus and spleen of allogeneically transplanted Balb/c mice. In f, g BALB/cJ recipient mice received 850 cGy of L-TBI. Within 48 hours post-radiation, mice were transplanted with allogeneic GFP 5×10^5 lineage depleted GFP BM cells + 10^6 GFP splenocytes. One group was simultaneously treated with the dual BMC. (h-l) Comparison of T-cell reconstitution in mice treated with BMC or OP9-DL1 derived pro-T-cells. Balb/cJ recipient mice received 850Gy L-TBI and were either provided OP9-DL1 culture derived 5×10^6 allogeneic GFP T-cell progenitors + 10^3 syngeneic HSCs or dual BMC + 5×10^5 lineage depleted allogeneic GFP BM cells. Total number of (h) DP and (i) SP4 and (j) SP8 thymocytes in the thymus and peripheral (k) $CD4^+$ and (l) $CD8^+$ T-cells in the spleen of transplanted mice 28 days post-transplant. Data in a-d are the mean ± s.d.of at n = 10 mice at the start of the study and are representative of 3 donors. Data in (e,g) and f are the mean ± s.d.of n = 7 and n=10 mice respectively and are representative of 2 independent experiments. Data in h-l are mean ± s.d. of n= 10 mice, representative of 2 independent experiments. Distinct samples were assayed individually. (*P < 0.05, ** P < 0.01, ***P < 0.001, analysis of variance (ANOVA) with a Tukey post hoc test).

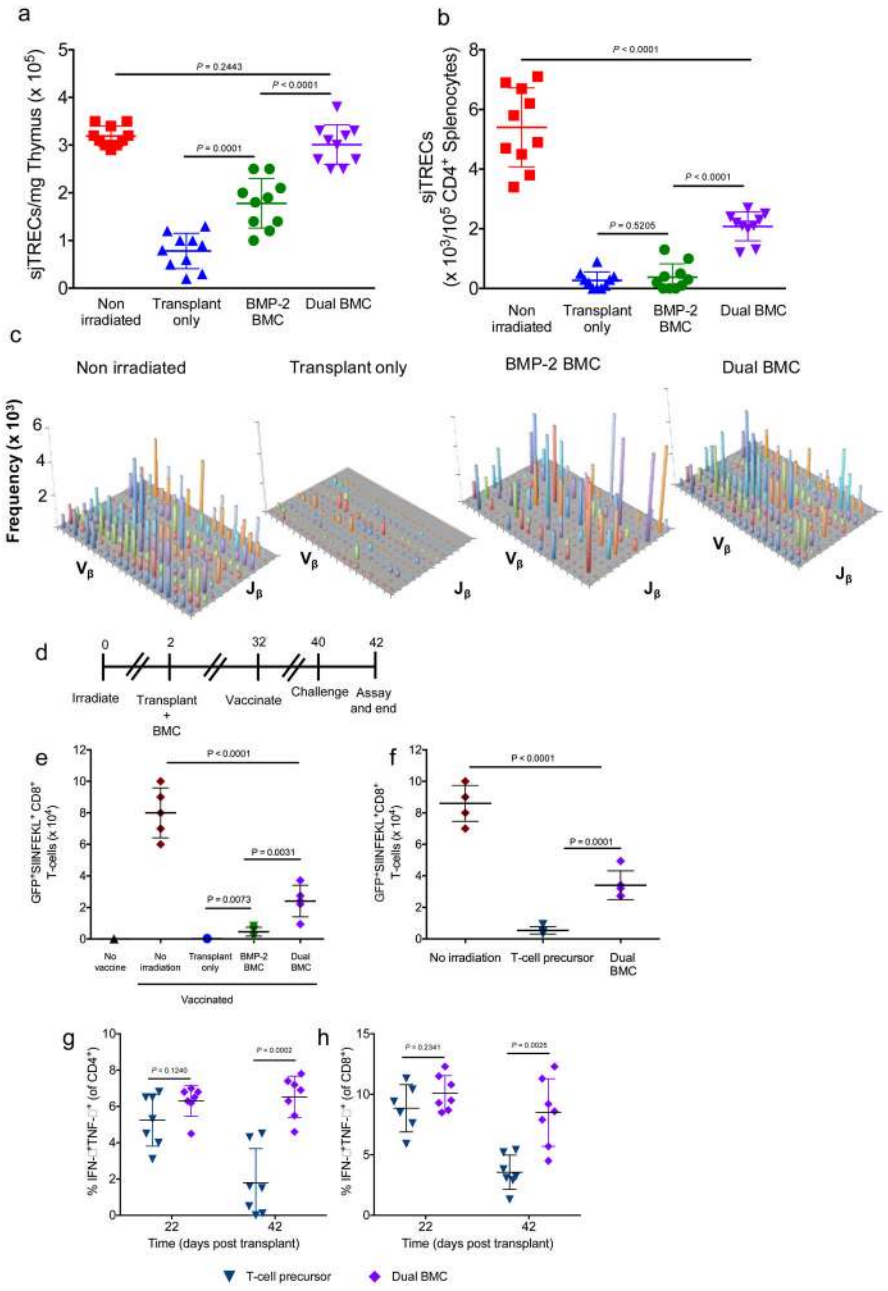

Figure 6.

Quantitative analysis of T-cell output, the immune repertoire and vaccination in mice with regenerated T-cells. T-cell receptor excision circle analysis from the (a) isolated thymus and (b) spleen in mice. (c) The diversity in antigen receptors of T-cells as analyzed by the sequenced V and J segments of the CDR3 beta chain in the BMC and transplant mice. Each bar represents a single clone. The plot provides depth (length of bar) and diversity (number of bars) of T-cells in the mice. Samples were pooled from five mice for each group and the combined data are represented. (d) Schedule of analyzing antigen-specific donor T-cell response through vaccination. (e) Donor SIINFEKL^{+}CD8^{+} T-cells enumerated in vaccinated mice after syn-HSCT and (f) allo-HSCT. (g, h) At day 22 and 42 after HSCT, splenocytes of

the OP9-DL1 T-cell precursor group and the dual-BMC treated group were stimulated and stained for surface markers and intracellular cytokines using antibodies specific for CD45.1, CD4, IFN-γ and TNF-α. Cells were gated on $CD4^+$ or $CD8^+$ donor cells, and analyzed for IFN-γ– and TNF-α–positive cells. In a-c and e, B6 recipients received 1000 cGy L-TBI and 5×10^5 lineage depleted syngeneic GFP BM cells. Post-HSCT mice with no BMC (Transplant only), post-HSCT mice treated with a BMP-2 BMC, and post-HSCT mice treated with a Dual BMC were analyzed and compared with non-irradiated mice that had not received a transplant or vaccine. In (f-h) Balb/cJ recipient mice received 850Gy L-TBI and were either provided OP9-DL1 culture derived 5×10^6 allogeneic GFP T-cell progenitors + 10^3 syngeneic HSCs or dual BMC + 5×10^5 lineage depleted allogeneic GFP BM cells. Data in a, b are mean ± s.d. of n = 10 mice, data in e, f are mean ± s.d. of n = 5 mice, data in (g, h) are mean ± s.d. of n = 7 mice. All experiments are representative of two independent experiments. (*P < 0.05, ** P < 0.01, ***P < 0.001, analysis of variance (ANOVA) with a Tukey post hoc test).